

Analysis of low saliency ratio and torque characteristics of the fractional slot concentrated winding surface mounted motors

HONGBO QIU, DONG WANG[✉], CUNXIANG YANG, KUN WANG

Zhengzhou University of Light Industry
Zhengzhou, Henan, China

e-mail: qiu_hongbo@zjhu.edu.cn / wangdong09042023@163.com

(Received: 07.09.2023, revised: 01.03.2024)

Abstract: In recent years, fractional slot concentrated winding permanent magnet synchronous motors (FSCW PMSMs) have become a hotspot in the research field. Due to the unique inductance characteristics of the FSCW PMSM, a fast and accurate calculation of the d/q -axis inductance and saliency ratio is necessary. In this paper, a method is proposed to calculate the d/q -axis reactance of the FSCW SPMSM, which constructs the equivalent magnetic circuit model of the d/q -axis armature reaction flux separately, and the saliency ratio characteristics of the FSCW SPMSM were demonstrated. In addition, to meet the high requirements of the modern industries, especially in servo systems, accurate consideration of the effect of stator resistance on torque and electromagnetic performance is important and more applicable. According to the relationship between the vector parameter, the explicit expression of the d/q -axis currents that consider the stator resistance is obtained, and the prediction of load angle at maximum electromagnetic torque is achieved. Then, combined with the finite element method, the influence mechanism of stator resistance on the motor steady-state performance is revealed. Finally, the experimental data are compared with the calculation data, and the correctness of the models and analysis was verified.

Key words: equivalent magnetic circuit model, inductance calculation, lower saliency ratio, torque characteristics



© 2024. The Author(s). This is an open-access article distributed under the terms of the Creative Commons Attribution-NonCommercial-NoDerivatives License (CC BY-NC-ND 4.0, <https://creativecommons.org/licenses/by-nc-nd/4.0/>), which permits use, distribution, and reproduction in any medium, provided that the Article is properly cited, the use is non-commercial, and no modifications or adaptations are made.

1. Introduction

Because of its short axial length, high efficiency, high torque density, and low cost, the fractional slot concentrated winding permanent magnet synchronous motor (FSCW PMSM) is widely used in servo systems, hybrid engines, electric vehicles, and low-speed direct-drive applications. It has gradually become the mainstream choice for middle and small motors [1–4]. The FSCW PMSM also has exhibited its advantages in sectors such as hybrid electric vehicles and wind energy applications [5–7].

Due to the special winding structure of the FSCW PMSM, the coupling between the phase windings is very low, and the wide stator teeth will lead to the high crossover of the q -axis and d -axis magnetic circuits, thus making the inductance characteristic of the FSCW PMSM different from that of the integral slot distributed winding (ISDW) PMSM [8–11].

Many scholars have done a lot of research on the inductance and the salient ratio of FSCW PMSMs.

Since the greater slot leakage inductance is beneficial to the expansion of the field weakening range, in [12], B. Prieto has derived the expression of the slot leakage inductance of the FSCW motor with different winding layers. F. Wu *et al.* found that if only the second-order harmonic component of the winding self-inductance is considered, the third harmonic will be introduced in the coupling terms of d/q -axis and 0-axis, and this harmonic component is determined by the saliency ratio [13]. In [14], Z. Zhang studied a surface-inset permanent magnet motor with the FSCW, by establishing an analytical model containing five subdomains, the motor saliency ratio was investigated. Honda *et al.* concluded that the difference between the q -axis inductance and the d -axis inductance of the FSCW PMSM is smaller and the motor saliency ratio is also smaller. Compared with the ISDW PMSM, the q -axis inductance of the FSCW PMSM is more likely to increase, and they proposed a method to reduce the q -axis flux by segmenting the PMs radially [15].

In [16], to improve the torque density and field weakening capability of the PM machine for Electric Vehicles Traction Applications, the H-shaped PM motor and U-shaped PM rotor are proposed, the inductance feature and characteristic current FSCW PM machines are investigated.

A large number of studies and researches have proved that the saliency ratio of the FSCW PMSM is always smaller than that of the corresponding ISDW PMSM, regardless of single-layer winding or double-layer winding, surface-mounted or interior rotor structures [17–20]. However, the low saliency ratio of the FSCW SPMSM seems to be of little concern, and there have been no theoretical studies and quantitative analyses to explain this phenomenon.

In recent years, some studies on stator resistance have been done for real-time monitoring of motor operating conditions and faults [21,22]. But, the effect of stator resistance on the load-angle characteristics of PMSMs is still little noticed. It is usually assumed that stator resistance is much smaller than the reactance, and the effect of stator resistance on electromagnetic power and torque is often ignored, especially when analytical models or equivalent magnetic circuit models are used. This assumption is not reasonable in applications where the high accuracy is required. Particularly for small capacity motors, the motor stator resistance is large due to wire diameter and other factors. Considering the requirements for the steady-state performances as well as the overload capability of the motor, it is necessary to study the effect of stator resistance on the motor.

2. Analysis on reactance

2.1. Reactance calculation

As the concept proposed in reference [20], the area where a phase winding is continuously distributed is defined as the mechanical phase region. The stator of the FSCW PMSM can be treated as an ordered arrangement of several types of mechanical phase regions. For the FSCW PMSM, the winding coils are wound on separate stator teeth, so the mechanical phase region is related to the form of stator teeth distribution or winding distribution.

According to the principle of rotating motor operation, the axis of the resultant magnetomotive force will coincide with the axis of the magnetic field generated by the A-phase winding. At this time, if the d -axis is in the same direction as the axis of the A-phase magnetic field, the direction of the resultant magnetomotive force will be the same as the direction of the d -axis. Then, the A-phase armature reaction inductance will equal to the d -axis armature reaction inductance. The d -axis inductance can be obtained by calculating the permeance of the mechanical phase regions.

Due to the non-integer slot/pole ratio $Q_s/2p$ of the FSCW PMSM, the d -axis and q -axis magnetic circuits are asymmetric, and the less $Q_s/2p$ is close to an integer, the more pronounced this difference is. When $Q_s/2p$ is greater than 1.5 or less than 0.5, the winding factor is less than 0.866, and the motors with these types of slot-pole combination could not be widely used, so it is meaningless to study them. In this paper, two FSCW SPMSMs with 12-slots/8-poles and 12-slots/10-poles are selected as examples for study.

To simplify the calculation, the following assumptions are proposed:

1. The reluctance of the motor core is zero, and only the permeance of the permanent magnet and air gap are calculated.
2. Because the permeability of the permanent magnet is close to that of air, the permanent magnet shape of the 12-slot/8-pole motor is simplified.
3. The area where the stator teeth are aligned is chosen as the computed area of the magnetic circuit.

Figure 1 shows the structures of the two motors, and the main structural parameters of the motors are shown in Table 1.

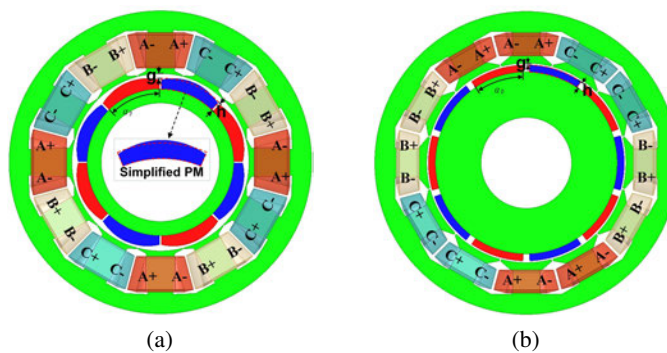


Fig. 1. Structure of the motors: (a) 8-pole/12-slot motor; (b) 10-pole/12-slot motor

For the 8-pole/12-slot motor, the path of flux generated by the A-phase armature reaction is shown in Fig. 2.

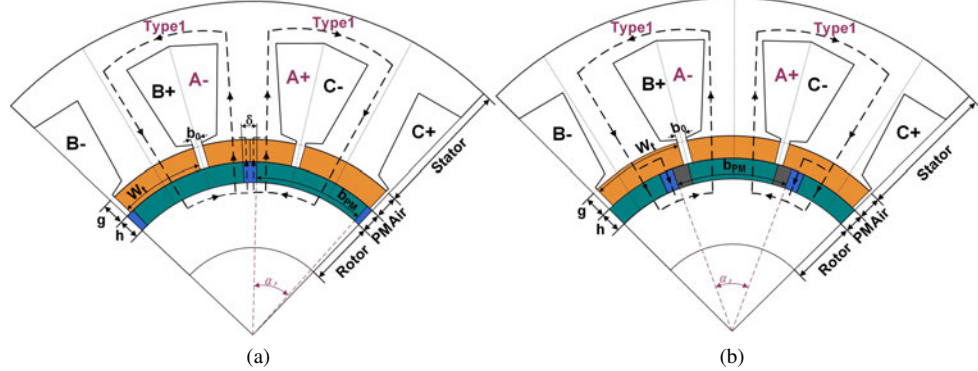


Fig. 2. Armature reaction flux path of the 8-pole/12-slot motor: (a) the *q*-axis path; (b) the *d*-axis path

Table 1. Main parameters of the motor

Parameter	8-pole/12-slot	10-pole/12-slot
Stator out diameter (mm)	72	167.2
Stator inner diameter (mm)	42.2	110
Rotor out diameter (mm)	34.85	100.2
Air-gap length (mm)	1.065	1
PM thickness (mm)	2.61	3.9
Length (mm)	50.8	130
Slot width (mm)	0.2	0.9
Winding turns	62	32
Frequency (Hz)	200	125
Pole-arc coefficient	0.97	0.887
Phase resistance (Ω)	2.7783	0.6552
Rated power (kW)	0.95	6.28
Rated current (A)	3.12	10.20
Rated voltage (V)	112	220
Rated torque (N)	3.03	40.12

The area of the A-phase is composed of only one mechanical phase region type, and the equivalent magnetic circuit models are shown in Fig. 3.

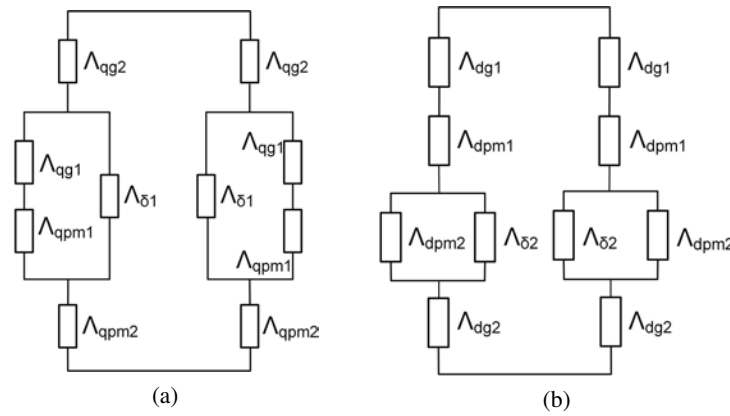


Fig. 3. Equivalent magnetic circuit models of the 8-pole/12-slot motor: (a) the q -axis magnetic circuit; (b) the d -axis magnetic circuit

There, $\Lambda_{\delta 1}$ is the permeance of half of the air region between the permanent magnets; $\Lambda_{\delta 2}$ is the permeance of the air region between the permanent magnets; Λ_{dg1} and Λ_{dg2} represent the permeances corresponding to the air gaps in different regions of the d -axis magnetic circuit, respectively; Λ_{qg1} and Λ_{qg2} represent the permeances corresponding to the air gaps in different regions of the q -axis magnetic circuit, respectively; Λ_{dpm1} and Λ_{dpm2} represent the corresponding permeabilities of permanent magnets in different regions of the d -axis magnetic circuit, respectively; Λ_{qpm1} and Λ_{qpm2} represent the corresponding permeabilities of permanent magnets in different regions of the q -axis magnetic circuit, respectively.

Assume that each phase area consists of n mechanical phase regions, with i slots in each mechanical phase region. The magnetic circuit permeances corresponding to each mechanical phase region are:

q-axis,

$$\Lambda_{qk} = \frac{1}{2} \frac{1}{\frac{\Lambda_{qg2}\Lambda_{qpgm2}}{\Lambda_{qg2} + \Lambda_{qpgm2}} + \frac{\Lambda_{qg1}\Lambda_{qpgm1}}{\Lambda_{qg1} + \Lambda_{qpgm1}} + \frac{1}{\Lambda_{\delta 1}}}, \quad (1)$$

d-axis,

$$\Lambda_{dk} = \frac{1}{2} \frac{1}{\frac{1}{\Lambda_{dg2}} + \frac{\Lambda_{dpm2}\Lambda_{\delta2}}{\Lambda_{dpm2}+\Lambda_{\delta2}}} + \frac{1}{\Lambda_{dg1}} + \frac{1}{\Lambda_{dpm1}}, \quad (2)$$

where Λ_{qk} and Λ_{dk} are the q -axis permeance and d -axis permeance for the k -th slot magnetic circuit in a mechanical phase region, respectively.

For the 10-pole/12-slot motor, the paths of the flux generated by the A-phase armature reaction are shown in Fig. 4.

It can be seen in Fig. 4, the area of the A-phase is composed of two mechanical phase region types, and due to the more complex magnetic circuit structure, the air gap region and permanent magnet region are divided into three regions, respectively. The equivalent magnetic circuit models are shown in Fig. 5.

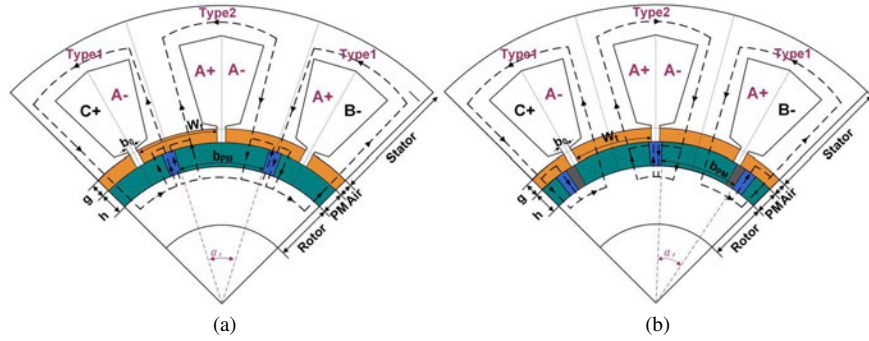


Fig. 4. Armature reaction flux path of the 10-pole/12-slot motor: (a) the *q*-axis path; (b) the *d*-axis path

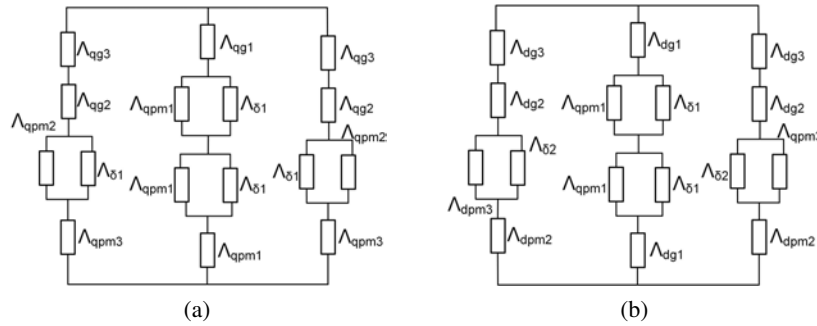


Fig. 5. Equivalent magnetic circuit model of the 10-pole/12-slot motor: (a) the *q*-axis circuit; (b) the *d*-axis circuit

The magnetic circuit permeances corresponding to each mechanical phase region are:
q-axis,

$$\Lambda_{qk} = \begin{cases} \frac{1}{2} \frac{\Lambda_{qg1} (\Lambda_{qpm1} + \Lambda_{\delta1})}{\Lambda_{qpm1} + \Lambda_{\delta1} + \Lambda_{\delta1}\Lambda_{qpm1}}, & k = \text{others} \\ \frac{1}{\frac{1}{\Lambda_{qg3}} + \frac{1}{\Lambda_{qpm3}} + \frac{\Lambda_{qg2} (\Lambda_{\delta1} + \Lambda_{qpm2})}{\Lambda_{qg2}\Lambda_{\delta1}\Lambda_{qpm2} + \Lambda_{qpm2} + \Lambda_{\delta1}}}, & k = 0/i \end{cases}, \quad (3)$$

d-axis,

$$\Lambda_{dk} = \begin{cases} \frac{1}{2} \frac{\Lambda_{dg1} (\Lambda_{dpm1} + \Lambda_{\delta1})}{\Lambda_{dpm1} + \Lambda_{\delta1} + \Lambda_{\delta1}\Lambda_{dpm1}}, & k = \text{others} \\ \frac{1}{\frac{1}{\Lambda_{dg2}} + \frac{1}{\Lambda_{dpm2}} + \frac{\Lambda_{dg3} (\Lambda_{\delta2} + \Lambda_{dpm3})}{\Lambda_{dg3}\Lambda_{\delta2}\Lambda_{dpm3} + \Lambda_{dpm3} + \Lambda_{\delta2}}}, & k = 0/i \end{cases}, \quad (4)$$

where Λ_{qk} and Λ_{dk} are the *q*-axis permeance and *d*-axis permeance for the *k*-th slot magnetic circuit in a mechanical phase region, respectively.

In the above analysis,

$$\begin{cases} \Lambda_{\delta 1} = \mu_0 l_{ef} \frac{\delta}{2h_{PM}}, \quad \Lambda_{\delta 2} = \mu_0 l_{ef} \frac{\delta}{h_{PM}} \\ \Lambda_{dgi} = \mu_0 l_{ef} \frac{w_i}{g}, \quad \Lambda_{dpmi} = \mu_0 \mu_r l_{ef} \frac{b_{PMi}}{h_{PM}} \end{cases}, \quad (5)$$

where: μ_0 is the permeability of air, μ_r is the relative permeability of the permanent magnets, h_{PM} is the thickness of the permanent magnets, δ is the width of the air region between the permanent magnets, g is the length of the air gap, b_{PMi} is the width of each segment of the permanent magnets, w_i is the width of each segment of the air gap, L_{ef} is the effective length of the motor core.

According to Eq. (6), the inductance of the closed magnetic circuit can be obtained.

$$L = N^2 \Lambda, \quad (6)$$

where: L is the inductance of one magnetic circuit, N is the turns of the coil which the magnetic flux coupled, Λ is the permeance of the magnetic circuit.

Thus, the total q -axis/ d -axis armature reaction inductances of each mechanical phase region are:

$$\begin{cases} L_{qn} = \sum_{k=1}^i N^2 \Lambda_{qk} \\ L_{dn} = \sum_{k=1}^i N^2 \Lambda_{dk} \end{cases}, \quad (7)$$

where i is the number of slots or teeth within each mechanical phase region.

The total armature reaction inductances of the motor are:

$$\begin{cases} L_{ad} = n \sum L_{dn} \\ L_{aq} = n \sum L_{qn} \end{cases}. \quad (8)$$

When the effect of periodic changes in armature current on the magnetic circuit saturation is neglected, the armature reaction inductance is only related to the magnetic circuit length as well as the material permeability. In the analysis below, it can be known that when the armature current is low, the saturation of the magnetic circuit is low, and the effect on the inductance is small, so the assumption in this section is feasible.

Due to the short end of the centralized winding, the end leakage reactance of the motor can be neglected, and the q -axis reactance and d -axis reactance can be obtained from Eq. (9):

$$\begin{cases} X_q = 2\pi f L_{aq} + X_s + X_h + X_c \\ X_d = 2\pi f L_{ad} + X_s + X_h + X_c \end{cases}, \quad (9)$$

where: X_q is the q -axis reactance, X_d is the d -axis reactance, f is the frequency, X_s is the slot leakage reactance, X_h is the harmonic leakage reactance, X_c is the tooth top leakage reactance. The calculation method of the leakage inductance can be found in [21].

From the above analysis, the results of the analytical method and the frozen permeability method are shown in Table 2.

As can be seen from Table 2, the saliency ratio of the surface-mounted permanent magnet motor with the FSCW is less than 1, and there are also differences in the saliency ratio with different slot-pole combinations, the saliency ratio of the 12-slot/8-pole motor is smaller than that of the 12-slot/10-pole motor.

Table 2. d/q -axis reactance and saliency ratio of the two motors

	Parameter	Equivalent magnetic circuit	FEM	Relative error
10/12	X_d	8.47	8.19	3.31%
	X_q	8.07	7.83	2.97%
	Saliency ratio	0.953	0.956	0.32%
8/12	X_d	13	13.54	4.15%
	X_q	12.26	12.4	1.14%
	Saliency ratio	0.943	0.916	2.86%

For the 12-slot/8-pole motor, the calculation results obtained by two methods have a larger relative error, the main reasons are the simplification of the permanent magnet shape, and the effect of the larger tooth top leakage.

2.2. Influence of the saliency ratio

When the permanent magnet motor runs stably in a certain state, the magnetic field generated by the permanent magnet will interact with the magnetic field generated by the armature reaction to produce a stable electromagnetic torque. If the d/q -axis magnetic circuit is asymmetrical, it will also cause a stable reluctance torque, and the output torque of the motor will be the synthesis of the two torques. The torque characteristic curves of the PMSM when the d/q -axis reactance is not equal are shown in Fig. 6.

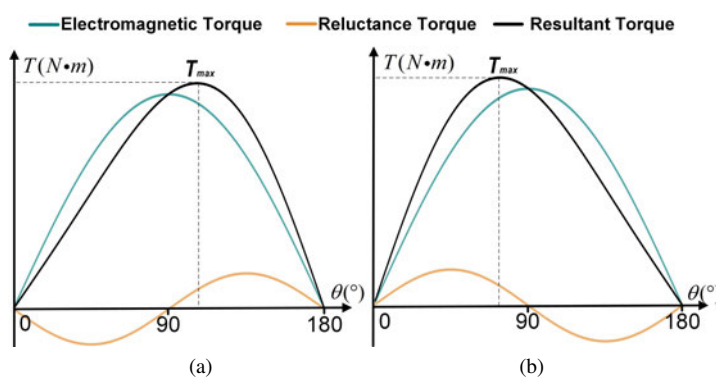


Fig. 6. Torque characteristic curve of permanent magnet motor: (a) $X_d < X_q$; (b) $X_d > X_q$

As can be seen in Fig. 6, for the FSCW SPMSM, because the saliency ratio is less than 1, the reluctance torque is a positive sinusoidal function as the load angle changes. The load angle is less than 90° when the motor output torque is maximum, which is a feature of this type of motor that has received less attention.

When the saliency ratio of the PMSM is not 1, and the maximum torque per ampere (MTPA) method is adopted, the current vector trajectories of the PMSM are as shown in Fig. 7. At most operating speeds, the trajectory of the maximum torque/per ampere ratio of the FSCW PMSM lies in the first quadrant.

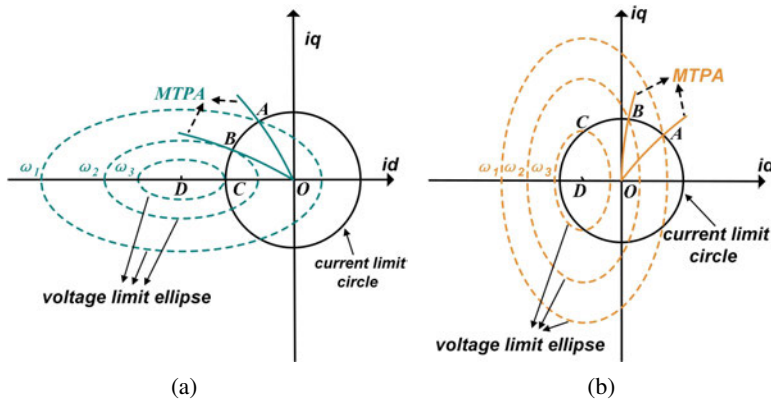


Fig. 7. Current vector trajectories of PMSM: (a) saliency ratio greater than 1; (b) saliency ratio less than 1

When the motor is running at low speed, the d -axis current with magnet excitation effect can be used to generate positive reluctance torque and improve the utilization rate of permanent magnets. When the motor is running at high speed, the air gap flux can be weakened by a relatively small d -axis current, the magnetic weaken performance of the motor can be effectively improved. In addition, the risk of irreversible demagnetization of the permanent magnet can be reduced, which improves the fault-tolerant performance of the motor and has significant advantages in control. Research based on the FSCW SPMSM characteristics is of great importance for the development of the negative-salient motor [22, 23].

3. Analysis of reactance

Conventionally, the stator resistance is often considered as the dependent variables of the motor winding structure to analyze motor electromagnetic properties, such as the flux linkage, but the effect of stator resistance on the power and the electromagnetic torque is often ignored. In many cases, this assumption will lead to many errors, especially for small servo motors, the stator phase resistance can reach 20% or more of the d -axis reactance, it is not rigorous or even feasible to ignore the effect of resistance. In this section, a 0.95 kW, 3 000 r/min FSCW SPMSM is taken as an example, taking into account the effect of stator resistance and saliency ratio, the motor performances are analyzed in detail.

3.1. Influence on load angle characteristics

When the stator resistance is different, the stable operating point of the motor is not the same. By establishing the vector diagram of the motor in the d/q coordinate system, the steady-state performance of the FSCW SPMSM can be further derived.

Figure 8 shows the typical phasor diagram of the FSCW SPMSM.

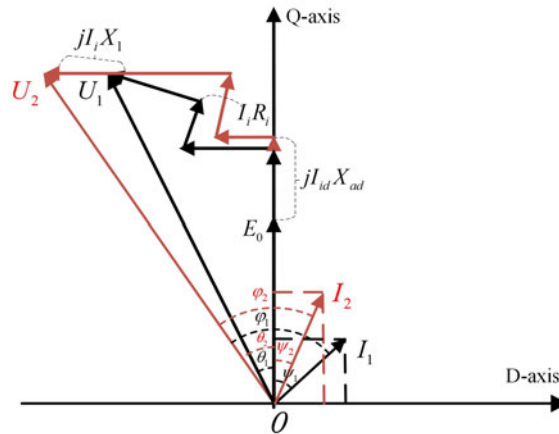


Fig. 8. Vector diagram of the FSCW SPMSM in d/q -axis coordinate system

E_0 and U are the no-load back electromotive force and input voltage of the machine, respectively; φ is the angle between the current and the input voltage, that is, the power factor angle; θ is the angle between the input voltage and the no-load back EMF, that is, the power angle; ψ is the angle between the current and the no-load back electromotive force, which is called the internal power factor angle. It can be seen from the figure that when the input voltage of the machine is constant, increasing the winding resistance will increase the armature current, and the power angle and internal power factor angle of the machine will also shift.

The explicit expressions for the q -axis and d -axis currents can be obtained according to the relationship between the parameters.

$$\begin{cases} i_q = \frac{[X_d U \sin \theta - R(E_0 - U \cos \theta)]}{(R^2 + X_d X_q)} \\ i_d = \frac{[R U \sin \theta - X_q (E_0 - U \cos \theta)]}{(R^2 + X_d X_q)} \end{cases} \quad (10)$$

The explicit expressions for the q -axis and d -axis currents can be obtained according to the relationship between the parameters.

According to conventional motor theory, the electromagnetic torque of the PMSM can be expressed as:

$$T_{em} = \frac{3p}{2\omega} i_q [E_0 + (X_d - X_q) i_d]. \quad (11)$$

To obtain the load angle when T_{em} is maximum, T_{em} can be considered as the function of θ , it can be assumed that:

$$T'_{em}(\theta) = \frac{3p}{2\omega} \left[i'_q(\theta) (E_O + (X_d - X_q) i_d) + i_q (X_d - X_q) i'_d(\theta) \right] = 0. \quad (12)$$

The expression for the load angle at maximum torque is:

$$\begin{aligned} & U \left(R^2 - X_d X_q \right) \cos 2\theta + R (X_d + X_q) U \sin 2\theta \\ & + \left(\frac{R^2 + X_d X_q}{X_d - X_q} R - R^2 + X_i X_q \right) E_0 \cos \theta - \left(\frac{R^2 + X_d X_q}{X_d - X_q} R + 2R X_q \right) E_0 \sin \theta = 0. \end{aligned} \quad (13)$$

Substituting the calculated reactance in Section 1 and the different resistances, the load angle at the maximum electromagnetic torque can be calculated by the analytical method and the finite element method, and the results are compared as follows (Table 3).

As the stator resistance decreases, the armature current rises significantly when the output torque is large, and the saturation of the magnetic circuit will increase, leading to the changes in reactance and saliency ratio, and increasing the deviations in the calculation results.

Figure 9 shows the variation of the q/d -axis reactance and saliency ratio with armature current amplitude and load angle. It can also be seen from the figure that although both the q -axis reactance and the d -axis reactance decrease when the current is higher, it is clear that the reactance is affected differently by the current and the current angle. When the current is small, the convex pole rate

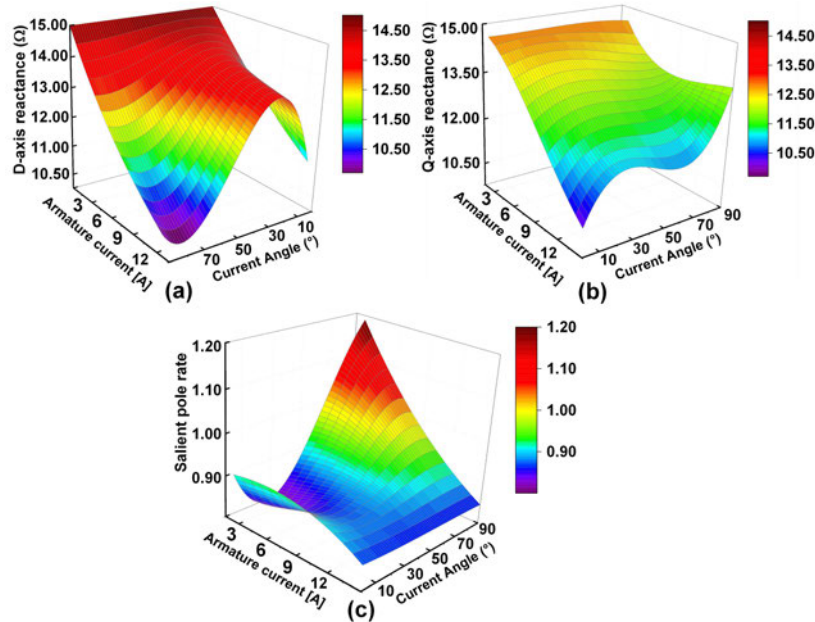


Fig. 9. The d/q -axis inductance and the saliency ratio according to the current and the current angle

changes with the current angle, while when the current is very high, the convex pole rate stays at a low value regardless of the current angle change, from which the nonlinear variation of the saliency ratio can be further obtained.

It can also be seen from Table 3 that the larger the stator resistance, the smaller the load angle at the maximum electromagnetic torque, it means that the overload capacity of the motor will be reduced.

Table 3. The load angle at maximum electromagnetic torque with different resistances

R (ohm)	0.1	0.5	1	2	2.7783	5
θT_{\max} by FEM	91.2	88.6	85.1	78.2	73.1	61.3
θT_{\max} by analytical method	85	83	81	76	73	64
Relative error	6.80%	6.32%	4.82%	2.81%	0.14%	-4.40%

3.2. Influence of resistance on motor steady-state performance

When the PMSM is running at no load, the magnetic field of the motor is established by the permanent magnets entirely, and the effect of the stator resistance on the parameters such as flux and no-load back-electromotive force can be ignored. When the PMSM is operated under load, the winding resistance will inevitably have an effect on the armature reaction, further leading to the changes in the performances of the motor.

When the stator resistance is different, not only the magnetic field distribution and the core saturation will have an impact on the core loss, the difference in the magnetic field harmonics and the current but also have an effect on the copper loss and the eddy current loss. Thus, the efficiency and power factor of the motor will also be affected.

In this section, the losses of the motor with different stator resistance are calculated by using the finite element method. Further, the effect of stator resistance variation on parameters such as efficiency and power factor of the motor has also been studied.

3.3. Influence of resistance at the same output power

To clarify the effect of the stator resistance on the steady-state performance of the PMSM, each performance is quantified at the same output power, losses are obtained, and compared in Fig. 10(a). The variations of efficiency, armature current, and power factor are presented in Fig. 10(b).

From Fig. 10(a), it can be seen that the larger the stator resistance, the smaller the core loss and eddy current loss, and with the resistance changes, the two losses have similar variation trends and the same rate of change. Compared with the case that stator resistance is 0.1Ω , when the stator resistance is 5Ω , the core loss and the eddy current loss are decreased by 26.6% and 28.54%, respectively.

The output power of the PMSM is proportional to the cross-product of the PM flux linkage and the current. From Fig. 10(b), it can be seen that with the gradual increase in stator resistance, the variation of armature current is within 15% when the output torque is constant. Meanwhile, the variation of copper loss shows an approximately linear variation with the change of resistance.

As can be seen from Fig. 10(b), the efficiency of the motor decreases as the loss gradually increases, but the power factor of the motor is gradually increased, because the copper loss is the active component. Compared to the case that the stator resistance is $0.1\ \Omega$, when the stator resistance is $5\ \Omega$, the power factor will increase by 7.55%, but the efficiency will decrease by 13.95%. Improving the efficiency and power factor is contradictory to changing the stator resistance.

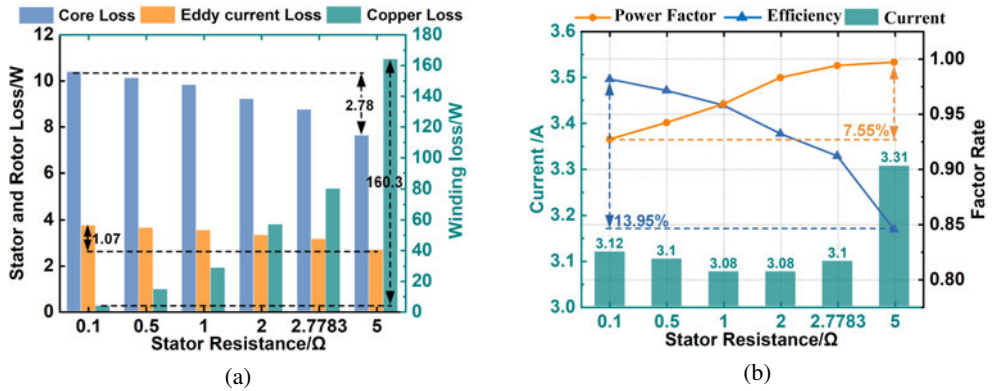


Fig. 10. The variation of motor performances with stator resistance at same output power: (a) losses; (b) current, efficiency, and power factor

In addition, with the resistance increasing, the current decreases and then increases. When the stator resistance is $1\ \Omega$, the armature current of the motor is the smallest, 3.08 A, and the efficiency and power factor are equal at this time.

3.4. Influence of resistance at the same load angle

The load angle is the angle between the stator magnetic field and the rotor magnetic field. When the load angle is constant and the motor is running steadily, the relationship between the various vectors will change as the stator resistance changes, and the motor performances also change. By using the finite element method, the effect of stator resistance on the motor performance is analyzed when the load angle is the same. The results are shown in Fig. 11.

From Fig. 11(a), it can be seen that when the load angle of the motor is constant, the torque and the current show a decreasing trend as the stator resistance increases. Compared with the case where the stator resistance is $0.1\ \Omega$, when the stator resistance is $5\ \Omega$, the electromagnetic torque and current decreased by 29.08% and 26.86%, respectively.

The reduction of current leads to the weakening of armature reaction, so the magnetic field strength will be reduced, and both core loss and eddy current loss show a slight decrease. Compared with the case that the stator resistance is $0.1\ \Omega$, when the stator resistance is $5\ \Omega$, the core loss and eddy current loss of the motor decreased by 2.34 W and 0.86 W, respectively. The change in copper loss and the change in resistance still show a linear relationship.

From Fig. 11(c), similar to the conclusion in Section 3.3, due to the increase in losses caused by the increase in resistance, the efficiency of the motor gradually decreases and the power factor gradually increases.

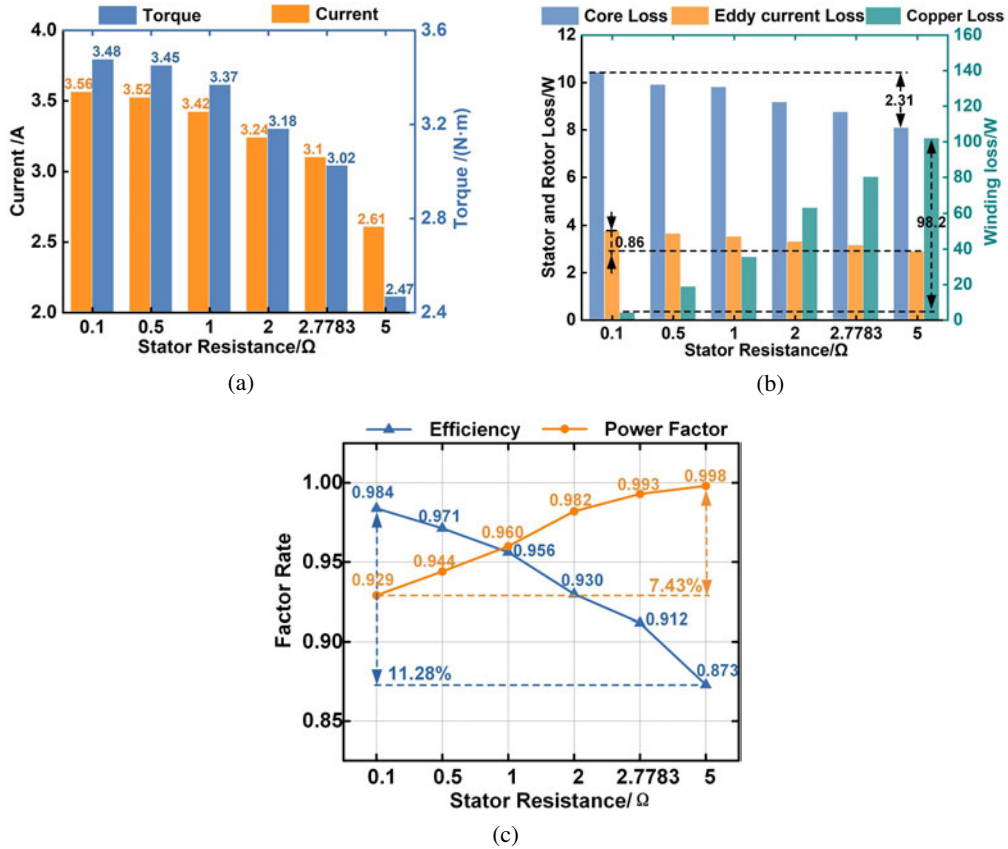


Fig. 11. The variation of motor performances with stator resistance at same output power: (a) current and torque; (b) losses; (c) efficiency and power factor

4. Figures and tables

In order to verify the accuracy of the calculation results, the 12-slot/8-pole, 0.95 kW motor is tested. During the experiment, different load torques are simulated by electromagnetic braking device, and the performance parameters and waveforms of the prototype in different states are recorded by the power analyzer. The experimental equipment used in the experiment mainly includes inverter power supply, experimental platform, 0.95 kW permanent magnet servo motor, power tester, magnetic control test bench (industrial condensing unit, Magtrol dynamometer machine, HIOKI PW6001 power analyzer), etc.

The motor operating temperature is at approximately 75° during the load test. The test platform and experimental equipment are shown in Fig. 12, and the various data are listed in Table 4, where the current refers to the rms of the phase current and the electromotive force is the rms of the phase voltage.

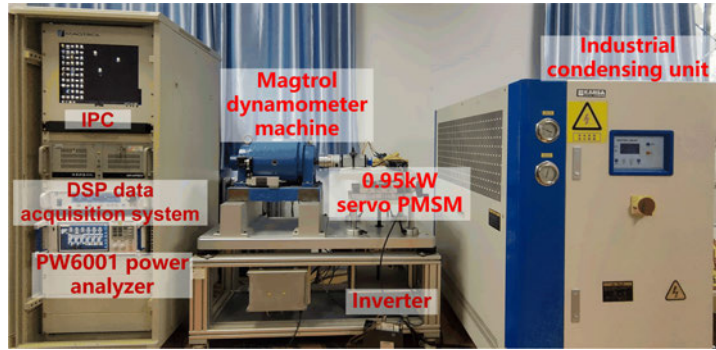


Fig. 12. Experimental test platform

It can be known from the table, the maximum error between the experimental data and calculated data is less than 5%. To further verify the accuracy of the model, the no-load back-EMF tested under low-frequency experiments is compared with the results obtained by using the finite element method.

Table 4. Comparison of calculated data and testing data

Operation	Parameter	Calculation data	Testing data	Relative error
No-load	EMF (V)	103.96	100.46	3.48%
0.95 kW	Current (A)	3.19	3.33	4.20%
	Power	98.84%	98.01%	0.83%
1.04 kW	Current (A)	3.45	3.31	4.23%

The back-EMF results obtained by the finite element model are not only close to the experimental ones in terms of RMS value but also agree well with the experimental waveforms (Fig. 13). Therefore, the accuracy of the finite element model and calculation results is guaranteed.

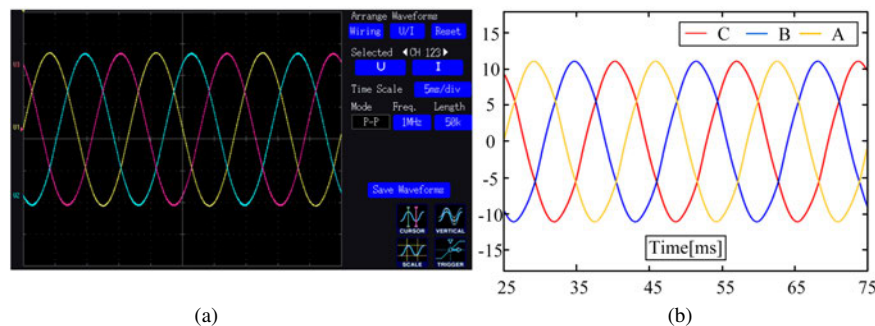


Fig. 13. Comparison of no-load back-EMF waveforms: (a) experimental test waveforms; (b) finite element method waveforms

5. Conclusions

This paper is aimed at the steady-state characteristic analysis of FSCW SPMSMs. The d/q -axis reactance is calculated by constructing an equivalent magnetic circuit model. On this basis, the effect of stator resistance is considered, and the torque characteristics and steady-state characteristics of the motor are analyzed. The conclusions are as follows:

1. Due to the structure of the FSCW PMSM, the q/d -axis magnetic circuit is asymmetric, the saliency ratio of FSCW SPMSM is less than 1. The less the slot/pole ratio is close to an integer, the smaller the saliency ratio is.
2. By establishing the equivalent magnetic circuit model, the accurate calculation of the q/d -axis reactance of the FSCW SPMSM can be obtained. Compared with the finite element results, the maximum calculation error of reactance is 4.15%. For the 10-pole/12-slot motor, the saliency ratio is 0.953. For the 8-pole/12-slot motor, the saliency ratio is 0.943. The main reasons for the calculation errors are the simplification of the permanent magnet shape and the effect of the tooth top leakage.
3. The load angle at maximum torque will change when the stator resistance is different. The larger the stator resistance is, the smaller the load angle at maximum torque is. When the stator resistance is $5\ \Omega$, the load angle at maximum torque is 61.3° , which is 29.9° less than that at $0.1\ \Omega$.
4. When the motor output power is constant, the greater the stator resistance, the smaller the core loss and the eddy current loss, the greater the copper loss. As the stator resistance increases, the power factor gradually increases, the efficiency gradually decreases, and the current first decreases and then increases. When the stator resistance is $1\ \Omega$, the armature current is the smallest, 3.0768 A, and the power factor and efficiency are equal, both are 0.958.
5. When the motor work angle is constant, the electromagnetic torque and current gradually decrease with increasing resistance. Compared with the case where the stator resistance is $0.1\ \Omega$, when the stator resistance is $5\ \Omega$, the electromagnetic torque and current of the motor decrease by 26.6% and 28.54%, respectively. Due to the increase in Joule loss on the winding, the power factor gradually increases and the efficiency gradually decreases as the stator resistance increases.

Acknowledgments

This work was supported in part by the National Natural Science Foundation of China under Grant U2004183, 52177063, and in part by Excellent Young Scholars Project of Henan Province under Grant 232300421070, and in part by the University Science and Technology Innovation Talent Support Program of Henan province under Grant 23HASTIT026, and in part by the Science and technology project of Henan Province under Grant 232102220080.

References

- [1] Zhenfei C., Hongzhong M., Jiayu L., Ning X., Zhixin L., *Armature MMF and electromagnetic performance analysis of dual three-phase 10-pole/24-slot permanent magnet synchronous machine*, Archives of Electrical Engineering, vol. 72, no. 1, pp. 189–210 (2023), DOI: [10.24425/aee.2023.143697](https://doi.org/10.24425/aee.2023.143697).

- [2] Wolnik T., Opach S., Cyganik Ł., Jarek T., Szekeres V., *Design methods for limiting rotor losses in a fractional slot PMSM motor with high power density*, Archives of Electrical Engineering, vol. 71, no. 4, pp. 963–979 (2022), DOI: [10.24425/aee.2022.142119](https://doi.org/10.24425/aee.2022.142119).
- [3] Hu L., Yang K., Sun S., Yu W., Ding Y., *Analysis of Characteristics of Permanent Magnet Synchronous Machines with Novel Topology of Fractional-Slot Concentrated Winding*, IEEE Transactions on Applied Superconductivity, vol. 30, no. 4, pp. 1–5 (2020), DOI: [10.1109/TASC.2020.2977587](https://doi.org/10.1109/TASC.2020.2977587).
- [4] Cai W., Wu X., Zhou M. et al., *Review and Development of Electric Motor Systems and Electric Powertrains for New Energy Vehicles*, Automot. Innov., vol. 4, pp. 3–22 (2021), DOI: [10.1007/s42154-021-00139-z](https://doi.org/10.1007/s42154-021-00139-z).
- [5] El-Refaie A.M., Zhu Z.Q., Jahns T.M., Howe D., *Winding Inductances of Fractional Slot Surface-Mounted Permanent Magnet Brushless Machines*, IEEE Industry Applications Society Annual Meeting, pp. 1–8 (2008), DOI: [10.1109/08IAS.2008.61](https://doi.org/10.1109/08IAS.2008.61).
- [6] Hebala A., Ghoneim W.A.M., Ashour H.A., *Detailed Design Procedures for PMSG Direct Driven by Wind Turbines*, J. Electr. Eng. Technol., vol. 14, pp. 251–263 (2019), DOI: [10.1007/s42835-018-00010-y](https://doi.org/10.1007/s42835-018-00010-y).
- [7] Min S.G., Sarlioglu B., *Analysis and Comparative Study of Flux Weakening Capability in Fractional-Slot Concentrated Windings*, IEEE Transactions on Energy Conversion, vol. 33, no. 3, pp. 1025–1035 (2018), DOI: [10.1109/TEC.2017.2781718](https://doi.org/10.1109/TEC.2017.2781718).
- [8] Wang Chengyu, Liu Chuang, Jiang Renhua, Zhang Jie, Ning Yinhang, *Effect of slot-and-pole combination on the flux-weakening properties of fractional-slot concentrated windings*, in Proc. Int. Conf. Elect. Mach. Syst., pp. 344–348 (2014), DOI: [10.1109/ICEMS.2014.7013510](https://doi.org/10.1109/ICEMS.2014.7013510).
- [9] Prieto B., Martínez-Iturralde M., Fontán L., Elosegui I., *Analytical Calculation of the Slot Leakage Inductance in Fractional-Slot Concentrated-Winding Machines*, IEEE Transactions on Industrial Electronics, vol. 62, no. 5, pp. 2742–2752 (2015), DOI: [10.1109/TIE.2014.2362094](https://doi.org/10.1109/TIE.2014.2362094).
- [10] Wu F., Ge H., EL-Refaie A.M., Farshadnia M., Pouramin A., Dutta R., *Partially-Coupled d-q-0 Components of Magnetically-Isolated FSCWIPM Machines with Open-End-Winding Drives*, IEEE Transactions on Industry Applications, vol. 56, no. 2, pp. 1397–1407 (2020), DOI: [10.1109/TIA.2020.2964251](https://doi.org/10.1109/TIA.2020.2964251).
- [11] Zhang Z., Xia C., Wang H., Shi T., *Analytical Field Calculation and Analysis of Surface Inset Permanent Magnet Machines with High Saliency Ratio*, IEEE Transactions on Magnetics, vol. 52, no. 12, pp. 1–12 (2016), DOI: [10.1109/TMAG.2016.2599147](https://doi.org/10.1109/TMAG.2016.2599147).
- [12] Honda Y., Nakamura T., Higaki T. et al., *Motor design considerations and test results of an interior permanent magnet synchronous motor for electric vehicles*, Industry Applications Conf., 1997, 32nd IAS Annual Meeting, IAS'97, Conf. Record of the 1997 IEEE, vol. 1, pp. 75–82 (1997), DOI: [10.1109/IAS.1997.643011](https://doi.org/10.1109/IAS.1997.643011).
- [13] Liu Y., Pei Y.L., Yu Y.J., Shi Y.W., Chai F., *Increasing the saliency ratio of fractional slot concentrated winding interior permanent magnet synchronous motors*, IET Electric Power Application, vol. 9, no. 7, pp. 439–448 (2015), DOI: [10.1049/iet-epa.2014.0336](https://doi.org/10.1049/iet-epa.2014.0336).
- [14] El-Refaie A.M., Jahns T.M., McCleer P.J., McKeever J.W., *Experimental verification of optimal flux weakening in surface PM Machines using concentrated windings*, IEEE Transactions on Industry Applications, vol. 42, no. 2, pp. 443–453 (2006), DOI: [10.1109/TIA.2006.870043](https://doi.org/10.1109/TIA.2006.870043).
- [15] Chong L., Rahman M.F., *Saliency ratio derivation and optimisation for an interior permanent magnet machine with concentrated windings using finite-element analysis*, IET Electr. Power Appl., pp. 249–258 (2010), DOI: [10.1049/iet-epa.2009.0119](https://doi.org/10.1049/iet-epa.2009.0119).
- [16] Tangudu J.K., Jahns T.M., EL-Refaie A., *Unsaturated and saturated saliency trends in fractional-slot concentrated-winding interior permanent magnet machines*, 2010 IEEE Energy Conversion Congress and Exposition, pp. 1082–1089 (2010), DOI: [10.1109/ECCE.2010.5617855](https://doi.org/10.1109/ECCE.2010.5617855).

- [17] Tong W.M., Wu S.N., An Z.L., *Study on the Inductance of Permanent Magnet Synchronous Machines with Fractional Slot Concentrated Winding Based on the Winding Function Method*, Transactions of China Electrotechnical Society, vol. 30, no. 13, pp. 150–157 (2015), DOI: [10.19595/j.cnki.1000-6753.tces.2015.13.020](https://doi.org/10.19595/j.cnki.1000-6753.tces.2015.13.020).
- [18] Cabrera L.A., Elbuluk M.E., Husain I., *Tuning the stator resistance of induction motors using artificial neural network*, IEEE Transactions on Power Electronics, vol. 12, no. 5, pp. 779–787 (1997), DOI: [10.1109/63.622995](https://doi.org/10.1109/63.622995).
- [19] Antonello R., Ortombina L., Tinazzi F., Zigliotto M., *Online Stator Resistance Tracking for Reluctance and Interior Permanent Magnet Synchronous Motors*, in IEEE Transactions on Industry Applications, vol. 54, no. 4, pp. 3405–3414 (2018), DOI: [10.1109/TIA.2018.2819961](https://doi.org/10.1109/TIA.2018.2819961).
- [20] Holakooie M.H., Ojaghi M., Taheri A., *Direct Torque Control of Six-Phase Induction Motor with a Novel MRAS-Based Stator Resistance Estimator*, in IEEE Transactions on Industrial Electronics, vol. 65, no. 10, pp. 7685–7696 (2018), DOI: [10.1109/TIE.2018.2807410](https://doi.org/10.1109/TIE.2018.2807410).
- [21] Renyuan Tang et al., *Modern permanent magnet motors: theory and design*, China Machine Press Bei Jing, China (1997).
- [22] Qiu H.B., Zhao X.F., Wei Y.Q., Ran Y., Yang C.X., *Influence of inter-turn short-circuit fault on the loss of high-speed permanent magnet generator with Gramme ring windings*, IET Electric Power Application, vol. 12, no. 5, pp. 1256–1262 (2019), DOI: [10.1049/iet-pel.2018.6097](https://doi.org/10.1049/iet-pel.2018.6097).
- [23] Safa H.H., Ebrahimi M., Zarchi H.A. et al., *Eccentricity fault detection in permanent magnet synchronous generators using stator voltage signature analysis*, Int. J. Precis. Eng. Manuf., vol. 18, pp. 1731–1737 (2017), DOI: [10.1007/s12541-017-0201-6](https://doi.org/10.1007/s12541-017-0201-6).